Substitutional tuning of electronic phase separation in CaFe3O5

Substitutional tuning of electronic phase separation in $CaFe_3O_5$

Ka H. Hong,[1] Elena Solana-Madruga,[1] Branislav Viliam Hakala,[1] Midori Amano Patino,[2] Pascal Manuel,[3] Yuichi Shimakawa,[2] and J. Paul Attfield[1]

[1]*Centre for Science at Extreme Conditions and School of Chemistry, University of Edinburgh, Mayfield Road, Edinburgh EH9 3FD, United Kingdom*

[2]*Institute for Chemical Research, Kyoto University, Uji, Kyoto 611-0011, Japan*

[3]*STFC Rutherford Appleton Lab, ISIS Facility, Harwell Science and Innovation Campus, Didcot, OX11 0QX, United Kingdom*

(Received 13 November 2020; accepted 26 January 2021; published 15 February 2021)

Electronic phase separation into charge-ordered (CO) and charge-averaged (CA) phases in $CaFe_{3-x}M_xO_5$ samples for dopants $M =$ Mn and Co has been investigated using powder neutron and x-ray diffraction, magnetization, and Mössbauer spectroscopy measurements. Electronic phase separation is observed in lightly doped $CaFe_3O_5$ samples, where 4–10% Ca is replaced by Mn, Fe, or Co, and the CA ground state is stabilized at higher doping levels. The CO and CA phases are found to emerge below a common magnetic ordering temperature at 300–320 K providing strong evidence for a lattice strain-driven mechanism that couples their magnetic transitions.

DOI: 10.1103/PhysRevMaterials.5.024406

I. INTRODUCTION

Coupling between spin, charge, and orbital degrees of freedom in iron oxides has been of great interest due to the complex ground state of magnetite, Fe_3O_4, where Fe^{2+}/Fe^{3+} charge order leads to direct Fe-Fe interactions within orbital molecule clusters of linear Fe trimerons when cooled below the Verwey transition at 125 K [1,2]. Recently, new members of the Fe_nO_{n+1} family have been discovered using high-pressure and high-temperature (HPHT) synthesis techniques [3,4], and these also display remarkable electronic behaviors. Structural studies of Fe_4O_5 and Fe_5O_6 revealed Fe dimers and trimers formed through charge and orbital orderings, accompanied by structural transitions, similar to the Verwey transition in Fe_3O_4 [5–7]. Several substituted MFe_3O_5 derivatives of Fe_4O_5 have also been reported. $MnFe_3O_5$ and $CoFe_3O_5$, made under HPHT conditions, exhibit a rich variety of magnetically ordered states when cooled below upper spin-ordering transitions near 350 K [8–10]. $CaFe_3O_5$, which can be prepared at ambient pressure, is of particular interest as a host system for electronic phase separation.

A previous investigation of an off-stoichiometric sample of $CaFe_3O_5$ with composition $Ca_{0.96}Fe_{3.04}O_5$ (labeled $x_{Fe} = 0.04$ for comparison with other doped samples in this paper) discovered that the high-temperature (HT) phase separates into long-range ordered charge-ordered (CO) and charge-averaged (CA) phases, with both the CO and CA phases sharing a magnetic ordering transition at $T_M = 302$ K [11]. The CO and CA phases both preserve the orthorhombic *Cmcm* symmetry of the HT $CaFe_3O_5$ structure [Fig. 1(a)]. This has three distinct cation sites: a trigonal prismatic site occupied by Ca^{2+} and two octahedrally coordinated Fe positions, with a 1:2:1 ratio of Ca:Fe1:Fe2 sites. Fe^{2+}/Fe^{3+} charge ordering and Fe^{2+} orbital ordering in the CO phase, with formal charge distribution $CaFe1^{3+}{}_2Fe2^{2+}O_5$ [Fig. 1(b)], lead to the formation of trimerons as observed in magnetite [2], whereas the CA phase has averaging of Fe^{2+}/Fe^{3+} charges as $CaFe1^{2.67+}{}_2Fe2^{2.67+}O_5$ [Fig. 1(c)] with no orbital order or trimeron formation. A subsequent study of stoichiometric ($x = 0$) $CaFe_3O_5$ found only the CO phase was formed below a magnetic transition at $T_M = 289$ K, with an incommensurate magnetic phase observed between T_M and 281 K [12].

Electronic phase separation has previously been of great interest in manganite perovskites where it gives rise to colossal magnetoresistances [13–15]. $CaFe_3O_5$ is notable as a non-perovskite system and furthermore displays separation into two electronically distinct phases with a shared T_M which is not found in manganites and is highly unusual. In this paper we have explored the substitutions of transition metals Mn and Co into $CaFe_3O_5$ in order to discover how systematic chemical doping changes structure, magnetic properties, and in particular the electronic phase separation.

II. EXPERIMENT

$CaFe_{3-x}M_xO_5$ samples with nominal $x_{Mn} = 0.10$, 0.25, and 0.50 and $x_{Co} = 0.05$, 0.10, and 0.50 compositions were prepared from stoichiometric proportions of $CaFe_2O_4$, Fe_2O_3, Fe, and MnO or CoO powders. These were mixed and ground, pressed into pellets, and heated at 1100 °C for 20 h in sealed evacuated quartz tubes. The precursor $CaFe_2O_4$ was prepared using a reported method [16], where $CaCO_3$ and Fe_2O_3 powders were ground together in 1:1 ratio, pressed into pellets, heated at 850 °C for 4 h, reground and repelleted, and finally reheated at 1100 °C for 12 h. Phase confirmation was carried out using a Bruker D2 powder x-ray diffractometer.

Magnetic measurements were carried out using a Quantum Design MPMS XL superconducting quantum interference

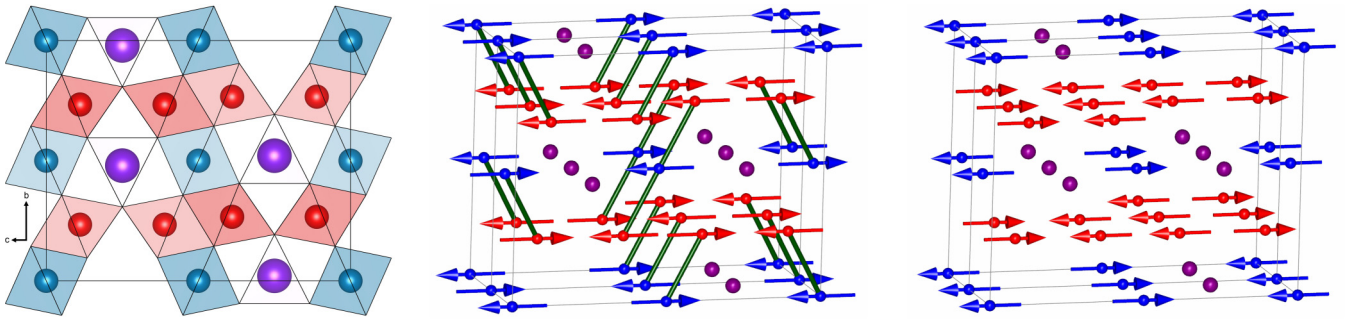

FIG. 1. (a) Projection of the $CaFe_3O_5$ structure showing FeO_6 octahedra for Fe1/Fe2 sites, and Ca ions within trigonal prismatic tunnels. (b) Magnetic structure of the CO phase with [½ 0 0] propagation vector, where lines show ferromagnetic order within trimerons [11]. (c) Magnetic structure of the CA phase, with [0 0 0] propagation vector. Fe1/Fe2 cations and spins are shown in red/blue and Ca ions are purple.

device magnetometer. The magnetic susceptibility of the samples was recorded between 2 and 400 K under field-cooled conditions, with an applied magnetic field of 1000 Oe.

Powder neutron-diffraction (PND) patterns were recorded at the WISH beamline of the ISIS spallation neutron source for the following samples and temperatures; $x_{Mn} = 0.10$ at 10−20 K, $x_{Mn} = 0.25$ at 150–320 K, $x_{Mn} = 0.50$ at 10 and 320 K, $x_{Co} = 0.05$ at 10 and 320 K, $x_{Co} = 0.10$ at 10–320 K, and $x_{Co} = 0.50$ at 10–320 K. The nuclear and magnetic structures were refined using the $CaFe_3O_5$ models [11] as a starting point, with magnetic k vectors = [½ 0 0] and [0 0 0] for the CO and CA phases, respectively. Powder synchrotron x-ray-diffraction (PSXRD) patterns were collected at the I11 beamline of the Diamond Light Source with incident wavelength 0.825 047 Å. The $x_{Mn} = 0.10$ and $x_{Co} = 0.50$ samples were packed in 0.5-mm glass capillaries and diffraction patterns were recorded from 100 to 350 K and 100 to 450 K, respectively. PND and PSXRD data were Rietveld fitted using the FULLPROF suite [17].

^{57}Fe Mössbauer spectroscopic measurements were performed in transmission geometry with a constant-acceleration spectrometer using a ^{57}/Co Rh radiation source. The velocity scale and the isomer shift (IS) were determined using the relative values of α-Fe at room temperature. 100-mg powder samples of the $x_{Fe} = 0.04$ [11] and $x_{Mn} = 0.10$ materials were placed into 1.5-cm-diameter coin-shaped capsules, made from 40 − μm-thick ultrapure aluminum foil. Spectra were recorded from the $x_{Fe} = 0.04$ sample at 3.5 K (91 h), 250 K (95 h), and 375 K (70 h), and from the $x_{Mn} = 0.10$ sample at the same temperatures with respective collection times of 117, 261, and 45 h. The spectra were fitted with Lorentzian functions using a least-squares method.

III. RESULTS

A. Powder neutron-diffraction analysis of high-temperature phases

Rietveld fits to PND patterns collected at 320 K confirmed the $CaFe_3O_5$-type structure with orthorhombic *Cmcm* space-group symmetry for all the samples. A representative fit is shown in Fig. 2. Trace amounts of brownmillerite ($Ca_2Fe_2O_5$)-type and spinel-type impurities were found in some samples as summarized in Ref. [18].

Refinements of the Mn or Co occupancy across the three cation sites making use of the high contrast in neutron scattering lengths between Ca, Fe, Mn, and Co (4.70, 9.45, −3.75, and 2.49 fm, respectively), evidence the introduction of Mn and Co into the $CaFe_3O_5$ structure as shown in Table I. Although $CaFe_{3-x}M_xO_5$ starting compositions were used with the intention of doping M = Mn and Co for Fe, the refinements show that M substitution is observed only at the Ca site at low contents ($x_M \leqslant 0.10$). This is surprising as Co, Fe, and Mn usually substitute for each other rather than Ca in metal oxides, but is consistent with the 4% Fe doping at the

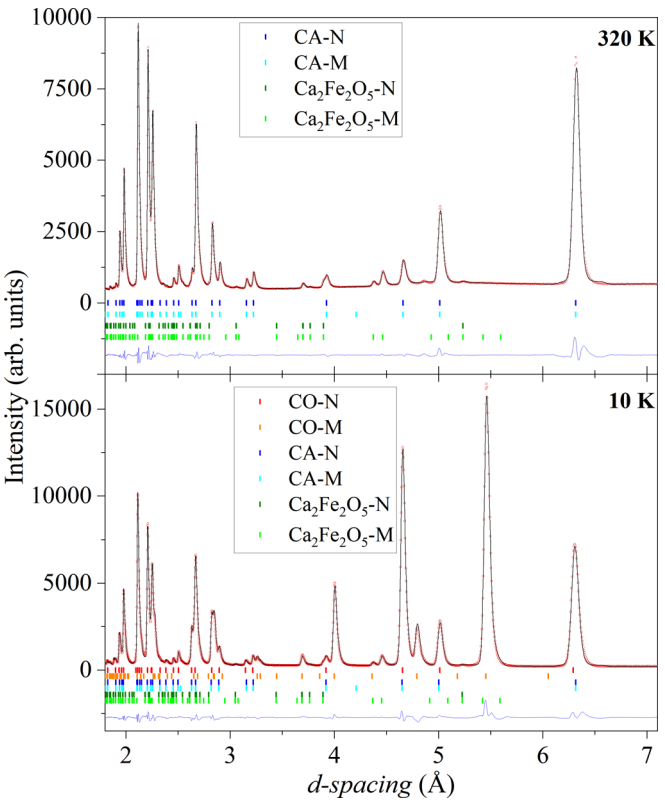

FIG. 2. Representative Rietveld fits to PND profiles, for the $x_{Co} = 0.05$ sample at 10 and 320 K. Bragg reflection marks from nuclear/magnetic phases shown are labeled N/M.

TABLE I. Occupancies at the three cation sites in doped $CaFe_3O_5$ samples from powder neutron refinements. Values for M = Mn and Co phases are from fits to 320 K data, and M = Fe is at 500 K [11]. Total compositions derived from these occupancies are also shown. Refined CO/CA phase fractions are from refinement against powder neutron or synchrotron x-ray (marked *) data at the lowest measured temperatures (neutrons: all M = Co samples and $x_{Mn} = 0.10$ and 0.50 at 10 K, $x_{Mn} = 0.25$ at 150 K, and $x_{Fe} = 0.04$ at 4 K [11]; x rays: $x_{Mn} = 0.10$ and $x_{Co} = 0.50$ at 100 K, and $x_{Fe} = 0.04$ at 80 K [11]).

M	x	Ca (Ca/M)	Fe1 (Fe/M)	Fe2 (Fe/M)	Overall composition	CO/CA
Mn	0.50	0.908/0.092(8)	0.858/0.142(2)	0.836/0.164(8)	$Ca_{0.908(8)}Mn_{0.540(12)}Fe_{2.552(9)}O_5$	0/1
	0.25	0.936/0.064(4)	0.95/0.05(2)	0.952/0.048(4)	$Ca_{0.936(4)}Mn_{0.212(6)}Fe_{2.852(5)}O_5$	0/1
	0.10	0.952/0.048(4)	1/0	1/0	$Ca_{0.952(4)}Mn_{0.048(4)}Fe_3O_5$	0.089/0.911(3), 0.069/0.931(2)*
Fe	0.04	0.960/0.040(8)	1/0	1/0	$Ca_{0.960(4)}Fe_{3.040(8)}O_5$	0.55/0.45(1), 0.759/0.241(3)*
Co	0.05	0.94/0.06(1)	1/0	1/0	$Ca_{0.94(1)}Co_{0.06(1)}Fe_3O_5$	0.622/0.378(8)
	0.10	0.92/0.08(2)	1/0	1/0	$Ca_{0.92(2)}Co_{0.08(2)}Fe_3O_5$	0.79/0.21(2)
	0.50	0.96/0.04(2)	0.954/0.046(2)	0.748/0.252(4)	$Ca_{0.96(2)}Co_{0.38(2)}Fe_{2.656(5)}O_5$	0.027/0.973(2), 0/1*

Ca site observed in the previous study of $CaFe_3O_5$ [11], so comparison of results across low-doped samples is appropriate. Substitution is also observed at Fe1 and Fe2 sites for larger amounts of Mn and Co. Comparison of site populations for the $x_M = 0.50$ samples in Table I shows that Mn occupies Fe1 and Fe2 sites almost equally, while Co has a clear preference for the Fe2 site. This suggests that Mn^{2+}/Mn^{3+} charge states are formed in a similar ratio to Fe^{2+}/Fe^{3+} within the host structure, whereas Co has a greater tendency to form the +2 state and occupy Fe2 sites (which are occupied by Fe^{2+} in the CO phase). The overall refined cation compositions in Table I are broadly consistent with the nominal values, although the refined 0.38(2) Co content is below the $x_{Co} = 0.50$ starting amount and chemical inhomogeneity in this sample is evidenced by PSXRD analysis below.

B. Magnetization measurements

Magnetization vs temperature measurements are shown in Fig. 3(a). All doped $CaFe_3O_5$ samples show a ferrimagnetic transition like that reported in $Ca_{0.96}Fe_{3.04}O_5$ [11] and other apparent transitions below 300 K in the Co-doped samples are due to the brownmillerite- or spinel-type impurities observed in the diffraction data. The magnetic transition temperature T_M increases with doping as shown in Fig. 3(b), from 289 K at $x = 0$ [12] to 302 K in the off-stoichiometric $x_{Fe} = 0.04$ sample, to 315 K for the upper explored Co-doping limit of $x_{Co} = 0.50$, and 330 K at the $x_{Mn} = 0.50$ upper Mn-doping value. This is surprising as substitution of Fe by Co or Mn in similar oxides generally decreases magnetic ordering temperatures, e.g., the Curie transition changes from 858 K for Fe_3O_4 to 789 K for $CoFe_2O_4$ [19] and 573 K for $MnFe_2O_4$ [20]. The unusual trend of T_M in doped $CaFe_3O_5$ samples is explained by a change in electronic ground state from the lower-T_M CO structure to the higher-T_M CA phase as the doping x_M increases, as evidenced from analysis of diffraction data below.

C. Powder neutron-diffraction analysis of low-temperature phases

PND patterns of the doped samples below T_M showed additional magnetic diffraction peaks characteristic of the previously reported charge-ordered CO ($\boldsymbol{k} = [1/2\ 0\ 0]$) or charge-averaged CA ($\boldsymbol{k} = [0\ 0\ 0]$) phases [Fig. 4(a)]. Fits to the PND data were carried out by simultaneously refining both the nuclear and magnetic structures, with cation site

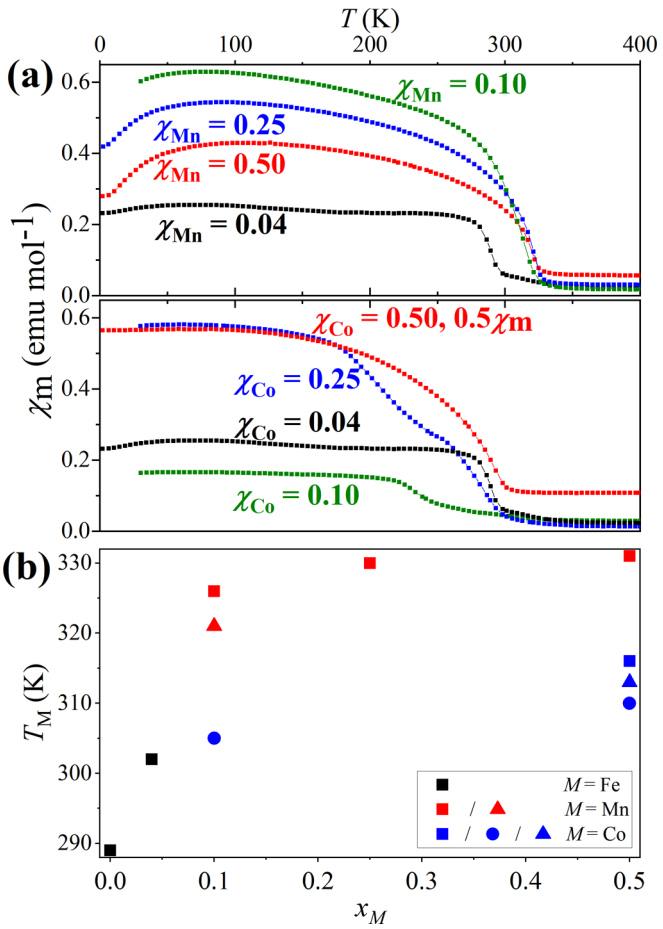

FIG. 3. (a) Thermal evolution of field-cooled magnetic susceptibility for doped $CaFe_3O_5$ phases. Data for the $x_{Co} = 0.50$ sample are scaled by 0.5 due to the presence of magnetic impurities. (b) Compositional evolution of the magnetic transition temperature T_M. Square/circle/triangle symbols represent values from magnetization/magnetic peak onset in PND/peak-width analysis of PSXRD. Data for $x = 0$ and $x_{Fe} = 0.04$ samples are, respectively, from Refs. [12] and [11].

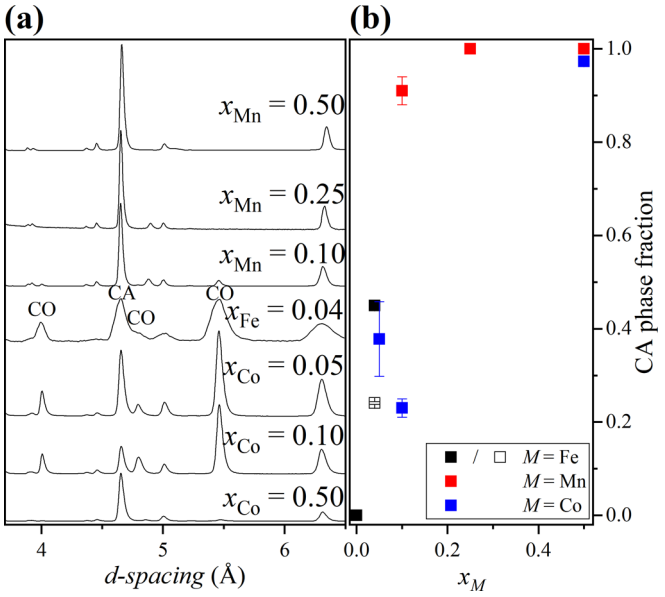

FIG. 4. (a) Comparison of PND data for doped $CaFe_3O_5$ samples at base temperatures (shown in Table I caption) with prominent magnetic peaks from the CO and CA phases labeled. All data are from the WISH diffractometer, except D2B data for $x_{Fe} = 0.04$ from Ref. [11]. (b) Base-temperature CA phase fractions refined against the PND data shown in (a) (closed symbols) or against PSXRD data (open symbols). Points for $x = 0$ and $x_{Fe} = 0.04$ samples are, respectively, from Refs. [12] and [11].

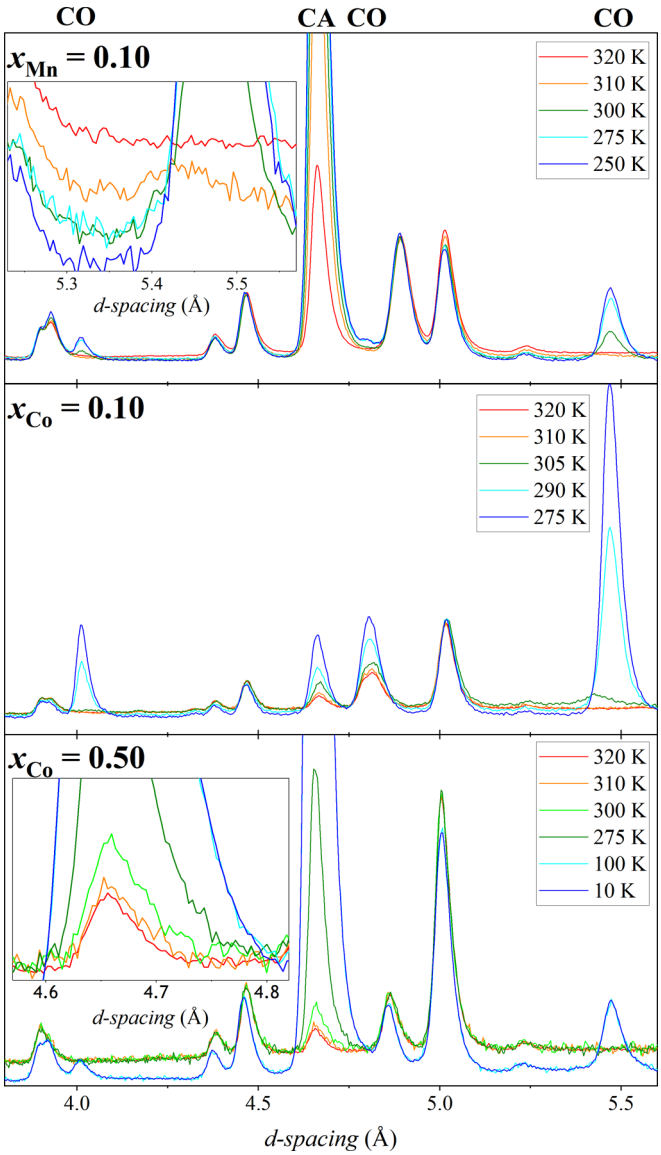

FIG. 5. Thermal evolution of magnetic scattering in PND profiles of three doped $CaFe_3O_5$ samples with prominent magnetic reflections from the CO and CA phases labeled at the top. $x_{Mn} = 0.10$ inset shows the appearance of a satellite peak at $d = 5.45$ Å from the incommensurate spin-ordered CO phase [12] between 300 and 320 K. $x_{Co} = 0.50$ inset panel highlights the growth of the magnetic CA reflection at $d = 5.45$ Å below 310 K.

occupancies fixed to the refined values obtained from analysis of the high-temperature data above. CO/CA phase fractions were also refined. Results are displayed in Figs. 1 and 4(b), Table I, and Ref. [18].

Plots of base-temperature PND patterns in Fig. 4(a) demonstrate that electronic phase separation is suppressed with increased doping, with the CA phase predominant at high doping levels. However, Co and Mn dopings behave rather differently as shown in Fig. 3(b). Co doping preserves substantial phase coexistence at low doping levels, with 38 and 23% CA phase observed, respectively, in $x_{Co} = 0.05$ and 0.10 materials at 10 K, comparable to the 45% CA observed in the $x_{Fe} = 0.04$ sample [11]. The $x_{Co} = 0.50$ sample is almost fully CA, and the observation of a residual 3% CO phase is likely due to chemical inhomogeneity as evidenced in analysis of the x-ray data for this phase below. Mn doping, by contrast, leads to a rapid suppression of the CO phase. The $x_{Mn} = 0.10$ sample has 91% CA phase at 10 K and no CO phase was detected for $x_{Mn} = 0.25$ and 0.50. Stabilization of the CA ground state at high Mn and Co dopings is also consistent with previous studies of the high-pressure phases $CoFe_3O_5$ and $MnFe_3O_5$, which may be viewed as $x_{Co} = 1$ and $x_{Mn} = 1$ compositions. Both showed $k = [000]$ magnetic structures similar to that of the CA phase of $CaFe_3O_5$, although with spin canting due to the additional presence of magnetic cations at the Ca site [8–10].

Hence this study demonstrates that electronic phase separation results from light doping of $CaFe_3O_5$. A stoichiometric $x = 0$ sample showed only the CO ground state [12]; samples with $0.04 \leqslant x_M \leqslant 0.10$ (M = Mn, Fe, Co) show substantial CO/CA electronic phase separation, and samples with $x_M \geqslant 0.10$ favor the CA ground state.

D. Variable-temperature powder neutron-diffraction analysis

An intriguing result from Ref. [11] was that the CO and CA phases in an $x_{Fe} = 0.04$ sample were found to emerge below a common magnetic ordering transition at $T_M = 302$ K. Thermal evolution of phase emergence for three samples, $x_{Mn} = 0.10$ and $x_{Co} = 0.10$ and 0.50, has thus been explored here and their PND profiles around T_M are shown in Fig. 5.

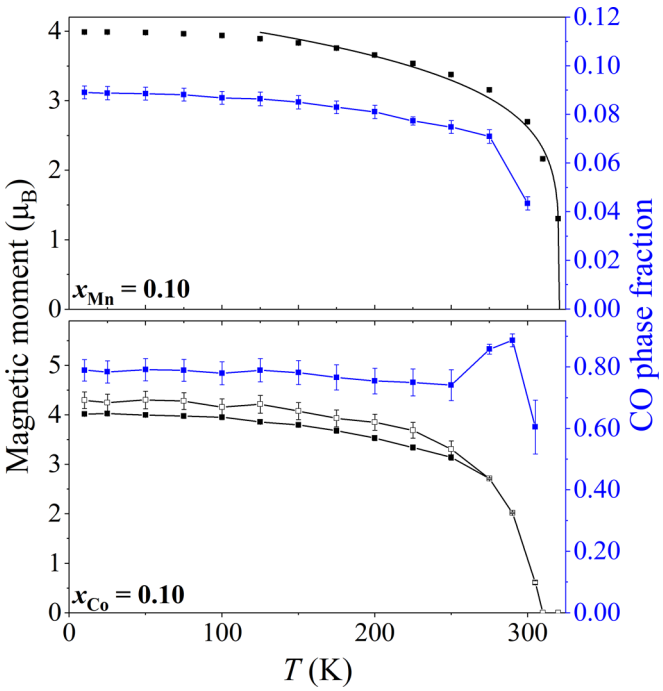

FIG. 6. Thermal evolution of the refined CO phase fraction and magnetic moments from fits to PND data for the $x_{Mn} = 0.10$ and $x_{Co} = 0.10$ samples between 10 and 320 K. A critical fit [19] to the magnetic moment of the $x_{Mn} = 0.10$ material between 125 and 320 K is shown [fitting parameters: $T_M = 320.5(4)$ K and $\beta = 0.19(1)$]. Other plotted lines are point to point. Closed/open symbols show magnetic moments from CO/CA phases of the $x_{Co} = 0.10$ sample.

For the $x_{Mn} = 0.10$ sample, both the strong CA magnetic peak at $d = 5.65$ Å and a weak satellite from the incommensurate magnetic CO phase [12] at $d = 5.45$ Å (shown in the inset to the $x_{Mn} = 0.10$ panel of Fig. 5) appear between 320 and 310 K, indicating that the CA and CO phases coemerge to within a few K. Magnetic order in the CO phase locks into the commensurate $k = [1/2\ 0\ 0]$ vector between 310 and 300 K. Magnetic moments at all Fe1 and Fe2 sites across both the CO and CA phases were constrained to have the same magnitude in fits to the data, as only ~9% of the CO phase is present. The resulting variations of magnetic moment and phase fraction are shown in Fig. 6. A critical fit (using the function shown in Ref. [21]) to the magnetic moments is shown in Fig. 6 and the fitted $T_M = 320.5(4)$K is consistent with the $T_M = 325$ K estimate from magnetization results above. The fitted critical exponent $\beta = 0.19(1)$ is between theoretical values for 2D ($\beta = 0.125$) and 3D ($\beta = 0.325$) Ising models. The CO/CA phase fractions show little thermal variation, and the apparent decrease around 300 K is likely an artifact of the constraint between CA and CO phase moments.

The $x_{Co} = 0.10$ sample also shows a coemergence of magnetic diffraction peaks from CO and CA phases, between 310 and 305 K, as evidenced by the profiles shown in Fig. 5. The incommensurate CO satellite peak near $d = 5.4$ Å is again observed just below T_M at 305 K but not at 290 K. In these fits it was possible to vary magnetic moments for the CO and CA phases independently for temperatures below 275 K, but the refined magnitudes differ little (Fig. 6). The CO/CA phase fractions vary little with temperature, other than showing some refinement instabilities as moments decrease approaching T_M.

The $x_{Co} = 0.50$ sample differs from the others in that different ordering temperatures are observed for the two spin structures. Peaks from the CA phase appear between 310 and 300 K, but those from the small (3%) CO fraction appear between 275 and 100 K. Further PND patterns were not collected in this interval and no further transition is evident in the magnetization data [Fig. 3(a)], but it is evident that the CA and CO spin-ordering transitions differ by at least 25 K for this sample. However, this is attributed to chemical inhomogeneity within the $CaFe_3O_5$-type phase as demonstrated by PSXRD analysis below.

Thermal evolution in the lattice parameters of the two low-temperature phases in the x_{Mn} and $x_{Co} = 0.10$ analogs (Fig. 7) below the magnetic ordering temperatures evidences anisotropic thermal expansion, as analyzed in Sec. G.

E. Powder synchrotron x-ray-diffraction analysis

PSXRD patterns were collected from the $x_{Mn} = 0.10$ and $x_{Co} = 0.50$ samples. Small amounts of $Ca_2Fe_2O_5$ and spinel-type impurities were observed [18]. A Rietveld fit to the $x_{Mn} = 0.10$ pattern at 350 K confirmed the high-temperature $CaFe_3O_5$-type structure with 5.6(1)% Mn substituting at the Ca site, in good agreement with PND analysis. The different lattice parameters for the CO and CA phases enable their structures to be refined independently against low-temperature PSXRD data. However, this was not possible for 300 and 310 K profiles where overlap of the two components was too great (and as x-ray diffraction does not observe the magnetic peaks that stabilize the two-phase PND refinements). However, the thermal variation of PSXRD diffraction peak widths [18] can be used to estimate $T_M = 321$ K, in good agreement with the values from PND phase analysis and the magnetic moment data in Fig. 6. Refined CO/CA phase fractions of 7%/93% at 100 K are also in good agreement with PND results above. Thermal evolution of lattice parameters is shown in Fig. 7.

PSXRD diffraction peaks for the $x_{Co} = 0.50$ sample also broaden below the magnetic transition, enabling $T_M = 313$ K to be estimated from a plot of peak width against temperature [18]. However, peaks in the high-temperature patterns showed a further anomalous broadening that could not be fitted well using a single-phase model. Two $CaFe_3O_5$-type components (labeled HT_1 and HT_2) were used to fit the high-temperature data, with corresponding CA_1 and CA_2 components below T_M (Fig. 8). The lattice parameters for the two phases diverge on cooling (Fig. 7), particularly below T_M, and do not vary in the same way as the CA/CO separation of lattice parameters observed for electronically phase-separated samples. The fraction of the HT_2 or CA_2 component is close to 25% from 100 to 450 K [18]. The maximal separation of CA_1 and CA_2 reflections in the lowest-temperature 100 K PSXRD pattern enabled their Ca site occupancies to be refined independently, and 7(1)% Co substitution for Ca was found for the CA_1 phase but none was observed for CA_2. These observations demonstrate that the $x_{Co} = 0.50$ sample is chemically inhomogeneous, with 75% of a Co-rich and 25% of a Co-poor

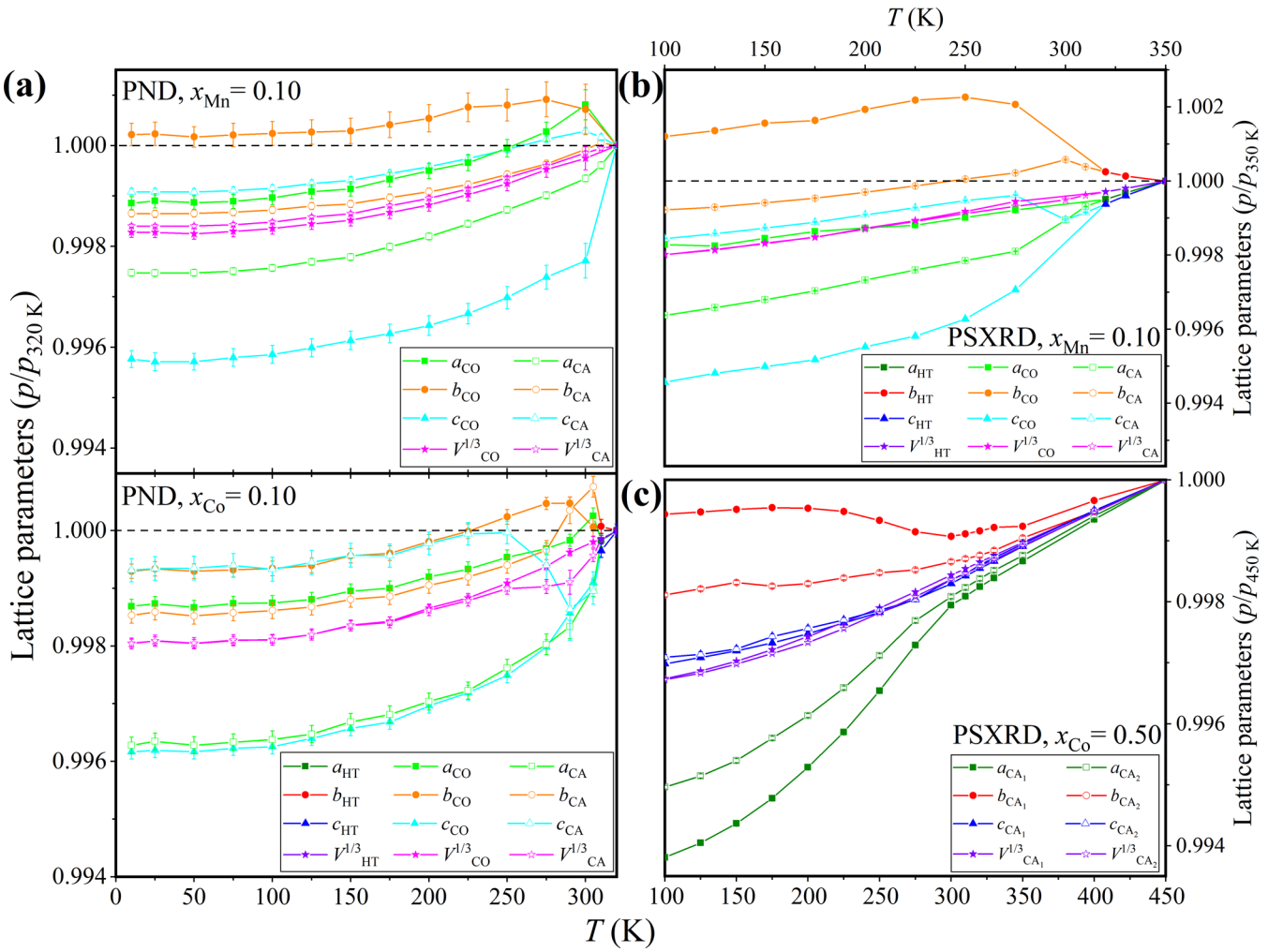

FIG. 7. Thermal variations of orthorhombic lattice parameters and volume in phase-separated doped $CaFe_3O_5$ samples, normalized to values at the highest measured temperature. (a) PND parameters for $x_{Mn} = 0.10$ [$a_{320K} = 3.0314(1)$ Å, $b_{320K} = 10.0158(5)$ Å, $c_{320K} = 12.6445(6)$ Å, and $V_{320K} = 383.90(3)$ Å^3] and $x_{Co} = 0.10$ [$a_{320K} = 3.0309(2)$ Å, $b_{320K} = 10.0162(8)$ Å, $c_{320\,K} = 12.6351(10)$ Å, and $V_{320K} = 383.58(5)$ Å^3] samples. (b) PSXRD parameters for the $x_{Mn} = 0.10$ sample [$a_{350K} = 3.032\,64(2)$ Å, $b_{350K} = 10.010\,65(7)$ Å, $c_{350K} = 12.650\,66(8)$ Å, and $V_{350K} = 384.057(4)$ Å^3]. Samples in (a) and (b) show electronic phase separation below $T_M = 300$–320 K. (c) PSXRD parameters for the $x_{Co} = 0.50$ material which is inhomogeneous or chemically phase-separated into two HT or CA phases at all temperatures [HT_1: $a_{450K} = 3.027\,92(3)$ Å, $b_{450K} = 10.0111(1)$ Å, $c_{450K} = 12.6524(1)$ Å, and $V_{450K} = 383.528(6)$ Å^3 and HT_2: $a_{450K} = 3.031\,86(7)$ Å, $b_{450K} = 10.0031(2)$ Å, $c_{450K} = 12.6539(4)$ Å, and $V_{450K} = 383.77(2)$ Å^3].

phase present. This may reflect some inhomogeneity introduced during the sample preparation procedure, or perhaps an intrinsic miscibility gap in the $CaFe_{3-x}Co_xO_5$ system. More work will be needed to clarify this aspect, but it is clear that the $x_{Co} = 0.50$ sample is chemically inhomogeneous and this likely accounts for the small (3%) CO phase observed with a spin-ordering transition well below T_M. No such chemical inhomogeneity is evidenced within the other doped-$CaFe_3O_5$ samples that show electronic phase separation.

F. Mössbauer spectroscopy

^{57}Fe Mössbauer spectra for $x_{Fe} = 0.04$ and $x_{Mn} = 0.10$ samples are, respectively, shown in Fig. 9 and Ref. [18] and fitting results are in Table II. Similar spectra were reported in an early study of $CaFe_3O_5$ [22]. Spectra for the HT phases at 375 K were fitted with two paramagnetic doublets in a fixed 2:1 intensity ratio representing the Fe1 and Fe2 sites. In both materials, a larger isomer shift for the Fe2 site reflects the slightly stronger occupancy preference for Fe^{2+} relative to the Fe1 site. The two sites have similar quadrupole splittings indicating comparable degrees of distortion in their octahedral environments.

Spectra collected below T_M were complex, exhibiting a collection of multiline components due to both magnetic order and electronic phase separation. The 250 K pattern of the $x_{Fe} = 0.04$ sample was fitted by a superposition of four sextets from the distinct Fe1 and Fe2 magnetic iron sites in each of the CO and CA phases. IS values of 0.46(1)/0.94(1)mm s^{-1} are found for the major component Fe1/Fe2 sextet pair [65(6)%], consistent with Fe^{3+} localization at the Fe1 site and Fe^{2+} at Fe2 site in the CO phase [23]. For the minor component Fe1/Fe2 sextet pair, the IS values are closer to each other as expected for charge averaging in the CA phase. The

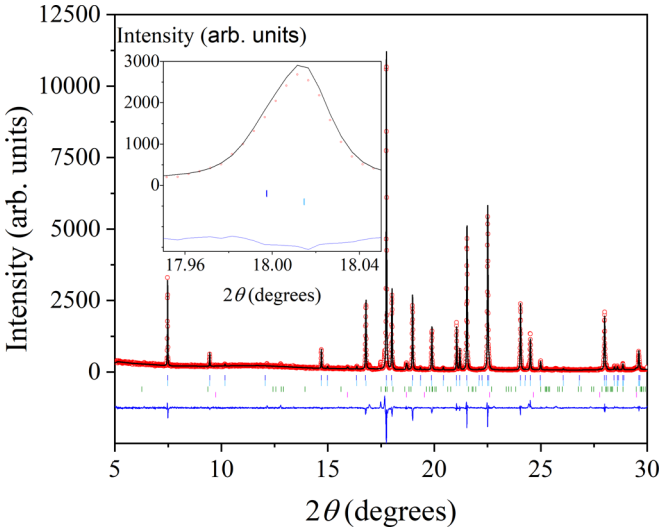

FIG. 8. Rietveld fit to PSXRD data for the $x_{Co} = 0.50$ sample at 450 K. Tick marks from top to bottom represent the HT_1, HT_2, $Ca_2Fe_2O_5$-, and spinel-type phases, respectively, and the inset shows the broadening of the (1 1 2) peak due to chemical separation of HT_1 and HT_2 phases.

separations between hyperfine (HF) magnetic splittings are also consistent with the charge-ordered and averaged natures of the two phases. Signals from the CA phase were largely masked by those from the dominant CO phase in the 3.5 K Mössbauer spectrum of the $x_{Fe} = 0.04$ sample. Hence the pattern was fitted using only two sextets to extract stable fitting parameters. The Fe1 and Fe2 site IS and HF values correspond to Fe^{3+} and Fe^{2+} states as observed for the CO phase at 250 K. The large errors obtained for the quadrupole shifts (QS) for the 3.5 and 250 K data show that these parameters are unstable likely due to overlapping of multiple sextet components in the spectra.

A well-resolved 250 K Mössbauer spectrum of the $x_{Mn} = 0.10$ sample was not obtained even after a long collection time (over 95 h), and this spectrum was not fitted. The 3.5 K spectrum was fitted with only two sextets and these have similar IS values consistent with the majority (>90%) CA phase observed in this sample.

Mössbauer thus provides a complementary spectroscopic method to the prior diffraction studies for observing long-range electronic phase separation in the $CaFe_3O_5$ system, and the measured isomer shift and hyperfine splitting values corroborate the Fe^{2+}/Fe^{3+} charge ordering within the CO phase and the charge averaging across Fe1 and Fe2 sites in the CA phase.

G. Lattice strains

The lattice parameters of the *Cmcm* CA and CO phases differ significantly, and their thermal variations shown in Fig. 7 are similar to those previously reported for the $x_{Fe} = 0.04$ sample [11]. To quantify these differences we calculate the interphase strain as $s_p = (p_{CA} - p_{CO})/p_{CO}$ for refined orthorhombic lattice parameters $p = a$, b, or c of the CA and CO phases. Values for the electronically phase-separated $CaFe_3O_5$ samples at the lowest measured temperatures are

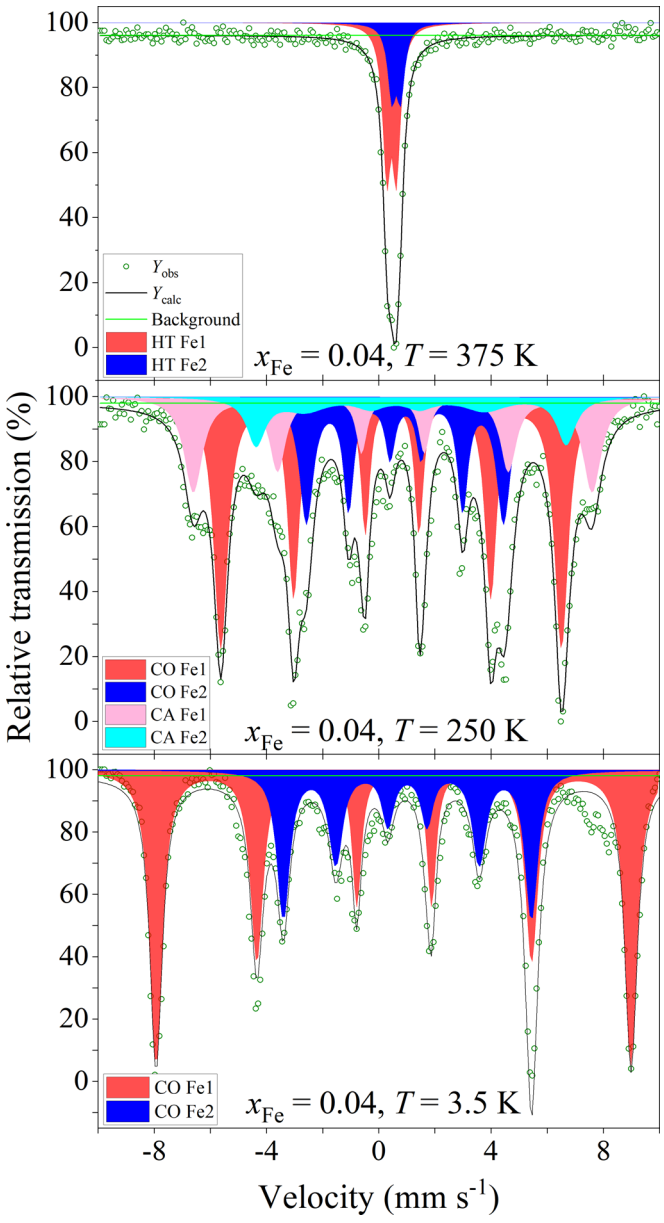

FIG. 9. Fitted Mössbauer spectra for the $x_{Fe} = 0.04$ sample at several temperatures showing signals from the Fe1 and Fe2 sites in the HT phase at 375 K, the electronically separated CO and CA phases at 250 K, and the CO phase alone at 3.5 K (the CA sextet could not be clearly resolved even after a long collection time).

shown in Table III. The base-temperature s_p values are very similar across all samples and they demonstrate that there is no significant interphase volume strain (i.e., $s_a + s_b + s_c \approx 0$ throughout), as also illustrated by the variations of unit-cell volume in the plots of Fig. 7. This, and the lack of any residual interphase strain above T_M for these samples (in contrast to the $x_{Co} = 0.50$ sample discussed above), indicates that there is no observed difference in chemical composition or valence electron concentration between the two components, as also observed for electronic phase separation in manganite perovskites. Any diffusion of transition-metal ions that might be driven by the phase separation would be negligible below the $T_M \sim 300$ K transitions, especially as samples were rapidly

TABLE II. Fitted Mössbauer parameters (isomer shift, hyperfine field, and quadrupole splitting of doublets at 375 K or quadrupole shift of sextets at 250 and 3.5 K) for the two iron sites in the $x_{Fe} = 0.04$ and the $x_{Mn} = 0.10$-doped $CaFe_3O_5$ samples.

M	*x*	*T* (K)	Phase	Site	IS (mm s^{-1})	HF (T)	QS (mm s^{-1})
Fe	0.04	375	HT	Fe1	0.46(1)	0	0.32(1)
				Fe2	0.62(1)	0	0.29(2)
		250	CO	Fe1	0.46(1)	37.6(1)	−0.04(1)
				Fe2	0.94(1)	21.8(1)	−0.02(2)
			CA	Fe1	0.51(2)	44.0(1)	−0.02(3)
				Fe2	0.79(12)	34.2(4)	0.71(24)
		3.5	CO	Fe1	0.54(1)	52.4(1)	−0.02(1)
				Fe2	1.02(1)	27.4(1)	−0.003(22)
Mn	0.10	375	HT	Fe1	0.40(1)	0	0.24(1)
				Fe2	0.73(2)	0	0.18(2)
		3.5	CA	Fe1	0.54(2)	52.2(1)	−0.08(4)
				Fe2	0.68(5)	30.5(2)	−0.50(10)

cooled to base temperatures of 4 or 10 K for PND studies, so it is a safe assumption that chemical composition is not changing in the electronically phase-separated regime.

The interphase strains in Fig. 7 show that the CA phase is contracted in the *a*- and *b*-directions, but expanded along *c*, relative to the CO structure. This is consistent with the ferromagnetic alignment of Fe spins leading to shortening of interatomic distances in sheets parallel to the *ab* plane in the CA phase, whereas these sheets have antiferromagnetic spin order in the CO structure. Trimeron formation in the CO phase shortens distances between sets of three successive *ab*-plane layers, resulting in the large contraction in the *c* axis (∼0.4%) relative to the CA structure.

H. Thermal history effects on electronic phase separation

Electronic phase separations mediated by lattice strain are sensitive to thermal history as repeated cooling and heating cycles tend to anneal samples towards the lowest-energy phase [24]. The $x_{Fe} = 0.04$ sample was first cooled to 4 K for a PND experiment [11], then heated to 500 K before cooling to and being stored at room temperature, close to $T_M = 302$ K. Portions of this sample were cooled a second time in separate PSXRD and Mössbauer experiments. The refined CO phase fractions obtained from fits to PND, PSXRD, and Mössbauer data at 250 K are 48(2), 62.8(3), and 65(6)%, respectively. The excellent agreement between second cooling (PSXRD and Mössbauer) results suggests that the increase in %CO after the first cooling for PND is due to thermal annealing towards this electronic phase as the lowest-energy state (as observed for $x = 0$ [12]), rather than an experimental artifact.

TABLE III. Interphase strains from electronic phase separation in doped $CaFe_3O_5$ samples, calculated using refined lattice orthorhombic parameters ($p = a$, *b,* or *c*) from fits to powder neutron or synchrotron x-ray- (*) diffraction profiles at the lowest measured temperatures shown. The CA phase fraction (from Table I) is also shown for reference. Data for $x_{Fe} = 0.04$ sample are from Ref. [11].

				s_p(%)		
M	*x*	*T* (K)	CA (%)	*a*	*b*	*c*
Mn	0.10	10	91	−0.14(1)	−0.15(2)	0.33(2)
		100	93	−0.20(1)*	−0.18(1)*	0.39(1)*
Fe	0.04	4	45	−0.159(1)	−0.237(1)	0.388(1)
		80	24	−0.156(1)*	−0.224(1)*	0.394(1)*
Co	0.05	10	38	−0.18(1)	−0.18(1)	0.36(1)
	0.10	10	21	−0.24(2)	−0.08(1)	0.32(2)

IV. DISCUSSION

The above results demonstrate that doping of $CaFe_3O_5$ is chemically complex. Although doping of M = Mn and Co at Fe sites was expected in $CaFe_{3-x}M_xO_5$ starting compositions, substitution is observed only at the Ca site for contents up to $x_M = 0.10$. This is consistent with the 4% self-doping of Fe at the Ca site observed in a previous study of $CaFe_3O_5$ [11], and with the complete replacement of Ca by transition metals in the high-pressure analogs Fe_4O_5, $MnFe_3O_5$, and $CoFe_3O_5$ [4,8,10]. Substitution of M = Mn and Co across all of the Ca, Fe1, and Fe2 sites is observed in $x_M \geqslant 0.10$ samples. Doping up to at least $x_{Mn} = 0.50$ is observed, but for the $x_{Co} = 0.50$ sample a chemical phase separation is observed which may have resulted from the sample preparation procedure, or may evidence a miscibility gap in the $CaFe_{3-x}Co_xO_5$ system.

Despite this chemical complexity, the electronic phase separation into CO and CA phases follows a consistent pattern across all the studied samples. Only the CO ground state is seen at $x = 0$ [12], substantial CO/CA electronic phase separation is observed in lightly doped samples ($0.04 \leqslant x_M \leqslant 0.10$ for M = Mn, Fe, and Co), and the CA ground state is stabilized at $x_M \geqslant 0.10$. The CO and CA ground states have very similar energies [11], and chemical disorder destabilizes the electronically ordered CO phase with respect to the electronically disordered or itinerant CA ground state.

The $x = 0$ CO phase has a magnetic (and charge, orbital, and trimeron) ordering transition at $T_M = 289$ K, whereas the highly doped CA phases have magnetic transitions at higher temperatures, $T_M \approx 310$ and 330 K, respectively, for Co and Mn. Hence, two magnetic transitions separated by 20–40 K might be expected in phase-separated samples. However, a striking feature is that the CO and CA phases are found to emerge below a common magnetic ordering

transition in all electronically phase-separated samples investigated. The variable-temperature powder neutron data show that the magnetic peaks from the two phases coemerge, to within experimental uncertainty of a few K, in the $x_{Fe} = 0.04$ [11], $x_{Mn} = 0.10$, and $x_{Co} = 0.10$ samples, at $T_M = 302$, 320, and 305 K, respectively. Such coemergence is not observed in electronically phase-separated manganites, where ordering temperatures for ferromagnetic and charge ordered phases are usually far apart. In $CaFe_3O_5$-based systems the two competing ground states have similar T_M′s, and we propose that this leads to a coupling between them via a lattice strain mechanism.

Results in Fig. 7 and Table III demonstrate that there are consistent lattice macrostrains associated with both CO and CA phases across all samples although the orthorhombic *Cmcm* symmetry does not change. Relative to the lattice parameters of the high-temperature phase extrapolated to below T_M, the CO phase has a small expansion in a, large expansion in b, and a large contraction in c, whereas the CA phase has a slight contraction in a, small expansion in b, and a small expansion in c. Cooling of a low-doped sample from the HT state would be expected to form the CA phase first with the CO ordering 20–40 K lower in the absence of strain effects, but the lattice strains created by initial nucleation of the CA phase evidently lead to both the CO and further CA phase emerging according to the local orientation of the orthorhombic domains within the polycrystalline sample. The growth of both phases leads to increasing strain fields through the sample that drives further CO or CA phase formation, so the whole HT sample transforms to a mix of CO and CA phases over a small temperature interval of ∼5 K, with no discernible difference between T_M′s for the two phases. The observed thermal annealing effect in the $x_{Fe} = 0.04$ sample further strengthens the case for a lattice strain coupling mechanism of electronic phase separation in doped $CaFe_3O_5$.

V. CONCLUSIONS

Electronic phase separation into charge-ordered and charge-averaged phases is shown to occur in lightly doped $CaFe_3O_5$ samples, where 4–10% Ca is replaced by Mn, Fe, or Co. Only the CO phase is observed below, and only the CA phase above, this doping range. The CO and CA phases are found to emerge below a common magnetic ordering temperature in phase-separated samples, and this is explained by a lattice strain-driven mechanism that leads to coupling of their magnetic transitions.

ACKNOWLEDGMENTS

We thank ERC and EPSRC for support, and STFC for provision of beam time at ISIS and the Diamond Light Source. This work was partly supported by grants for the International Collaborative Research Program of Institute for Chemical Research in Kyoto University from MEXT and the JSPS Core-to-Core Program (A) Advanced Research Networks, Japan.

[1] E. J. W. Verwey, Nature (London) **144**, 327 (1939).
[2] M. S. Senn, J. P. Wright, and J. P. Attfield, Nature (London) **481**, 173 (2011).
[3] B. Lavina, P. Dera, E. Kim, Y. Meng, R. T. Downs, P. F. Weck, S. R. Sutton, and Y. Zhao, Proc. Natl. Acad. Sci. USA **108**, 17281 (2011).
[4] B. Lavina and Y. Meng, Sci. Adv. **1**, e1400260 (2015).
[5] S. V. Ovsyannikov, M. Bykov, E. Bykova, D. P. Kozlenko, A. A. Tsirlin, A. E. Karkin, V. V. Shchennikov, S. E. Kichanov, H. Gou, A. M. Abakumov, R. Egoavil, J. Verbeeck, C. McCammon, V. Dyadkin, D. Chernyshov, S. van Smaalen, and L. S. Dubrovinsky, Nat. Chem. **8**, 501 (2016).
[6] S. V. Ovsyannikov, M. Bykov, E. Bykova, K. Glazyrin, R. S. Manna, A. A. Tsirlin, V. Cerantola, I. Kupenko, A. V. Kurnosov, I. Kantor, A. S. Pakhomova, I. Chuvashova, A. I. Chumakov, R. Rüffer, C. McCammon, and L. S. Dubrovinsky, Nat. Commun. **9**, 4142 (2018).
[7] S. V Ovsyannikov, M. Bykov, S. A. Medvedev, P. G. Naumov, A. Jesche, A. A. Tsirlin, E. Bykova, I. Chuvashova, A. E. Karkin, V. Dyadkin, D. Chernyshov, and L. Dubrovinsky, Angew. Chem. Int. Ed. **59**,5632 (2020).
[8] K. H. Hong, G. M. McNally, M. Coduri, and J. P. Attfield, Z. Anorg. Allg. Chem. **642**, 1355 (2016).
[9] K. H. Hong, A. M. Arevalo-Lopez, M. Coduri, G. M. McNally, and J. P. Attfield, J. Mater. Chem. C **6**, 3271 (2018).
[10] K. H. Hong, E. Solana-Madruga, M. Coduri, and J. P. Attfield, Inorg. Chem. **57**, 14347 (2018).
[11] K. H. Hong, A. M. Arevalo-Lopez, J. Cumby, C. Ritter, and J. P. Attfield, Nat. Commun. **9**, 2975 (2018).
[12] S. J. Cassidy, F. Orlandi, P. Manuel, and S. J. Clarke, Nat. Commun. **10**, 5475 (2019).
[13] E. Dagotto, T. Hotta, and A. Moreo, Phys. Rep. **344**, 1 (2001).
[14] M. Uehara, S. Mori, C. H. Chen, and S. W. Cheong, Nature (London) **399**, 560 (1999).
[15] Y. Tokura, Rep. Prog. Phys. **69**, 797 (2006).
[16] R. Wan, C. Jia, and W. Zhang, J. Alloy Compd. **544**, 1 (2012).
[17] J. Rodriguez-Carvajal, Physica B **192**, 55 (1993).
[18] See Supplemental Material at http://link.aps.org/supplemental/10.1103/PhysRevMaterials.5.024406 for further tables of results from PND and PSXRD refinements and figures showing further PND, PSXRD, and Mossbauer data and results plots.
[19] B. Liu, J. Ding, J. Yi, J. Yin, and Z. Dong, J. Korean Phys. Soc. **52**, 1483 (2008).
[20] G. U. Kulkarni, K. R. Kannan, T. Arunarkavalli, and C. N. R. Rao, Phys. Rev. B **49**, 724(R) (1994).
[21] M. S. Senn, J. P. Wright, J. Cumby, and J. P. Attfield, Phys. Rev. B **92**, 024104 (2015).
[22] R. Gerardin, E. Millon, J. F. Brice, O. Evrard, and G. Le Caer, J. Phys. Chem. Solids **46**, 1163 (1985).
[23] F. Menil, J. Phys. Chem. Solids,**46**, 763 (1985).
[24] S. K. Giri and T. K. Nath, J. Appl. Phys. **115**, 053902 (2014).